1521-0111/95/5/537–550$35.00
MOLECULAR PHARMACOLOGY

https://doi.org/10.1124/mol.118.115220
Mol Pharmacol 95:537–550, May 2019

Protocol-Dependent Differences in IC_{50} Values Measured in Human Ether-Á-Go-Go–Related Gene Assays Occur in a Predictable Way and Can Be Used to Quantify State Preference of Drug Binding [S]

William Lee, Monique J. Windley, Matthew D. Perry, Jamie I. Vandenberg, and Adam P. Hill

Victor Chang Cardiac Research Institute (W.L., M.J.W., M.D.P., J.I.V., A.P.H.) and St Vincent's Clinical School (W.L., M.J.W., M.D.P., J.I.V., A.P.H.), University of New South Wales, Darlinghurst, New South Wales, Australia

Received November 13, 2018; accepted February 10, 2019

ABSTRACT

Current guidelines around preclinical screening for drug-induced arrhythmias require the measurement of the potency of block of voltage-gated potassium channel subtype 11.1 (K_v11.1) as a surrogate for risk. A shortcoming of this approach is that the measured IC_{50} of K_v11.1 block varies widely depending on the voltage protocol used in electrophysiological assays. In this study, we aimed to investigate the factors that contribute to these differences and to identify whether it is possible to make predictions about protocol-dependent block that might facilitate the comparison of potencies measured using different assays. Our data demonstrate that state preferential binding, together with drug-binding kinetics and trapping, is an important determinant of the protocol dependence of K_v11.1 block. We show for the first time that differences in IC_{50} measured between protocols occurs in a predictable way, such that machine-learning algorithms trained using a selection of simple voltage protocols can indeed predict protocol-dependent potency. Furthermore, we also show that the preference of a drug for binding to the open versus the inactivated state of K_v11.1 can also be inferred from differences in IC_{50} values measured between protocols. Our work therefore identifies how state preferential drug binding is a major determinant of the protocol dependence of IC_{50} values measured in preclinical K_v11.1 assays. It also provides a novel method for quantifying the state dependence of K_v11.1 drug binding that will facilitate the development of more complete models of drug binding to K_v11.1 and improve our understanding of proarrhythmic risk associated with compounds that block K_v11.1.

Introduction

The voltage-gated potassium channel subtype 11.1 [K_v11.1 (or hERG (human ether-à-go-go-related gene))] carries one of the main repolarizing currents that contribute to the cardiac action potential—the rapid component of the delayed rectifier current (I_{Kr}) (Perrin et al., 2008b). Drugs that block K_v11.1 are the most common cause of acquired long QT syndrome, where drug-induced prolongation of repolarization can result in the fatal polymorphic cardiac arrhythmia torsade de pointes. As a result of these proarrhythmic side effects, a range of structurally unrelated drugs, including antihistamines, antibiotics, and antipsychotics were withdrawn from the market. In 2005, safety guidelines were put in place that mandated screening for K_v11.1 block for all new chemical entities to identify potentially proarrhythmogenic drugs during early preclinical development (Food and Drug Administration, HHS, 2005). Although these guidelines have been successful in preventing new proarrhythmic drugs unknowingly coming to market, this has come at the cost of an unnecessarily high attrition rate of drugs in development (Sager et al., 2014) (i.e., current safety guidelines are very sensitive but not very specific).

At the preclinical level, a safety margin is determined by comparing the electrophysiologically determined the IC_{50} of K_v11.1 to the C_{max} of the drug, where the closer these two values are, the higher the risk (Redfern et al., 2003). One criticism of current guidelines is that they do not specify what methods, including cell types, voltage protocols, and temperatures, should be used to measure IC_{50}. Several studies have demonstrated significant differences in measured IC_{50} values due to variations in all these factors (Kirsch et al., 2004; Yao et al., 2005; Milnes et al., 2010; Windley et al., 2018); in some cases, as much as a 60-fold difference in IC_{50} values was

This work was supported by the National Health and Medical Research Council of Australia (NHMRC) [Grant APP1088214]. W.L. is supported by a National Heart Foundation of Australia Health Professional Scholarship [APP101552]. J.I.V. is supported by a NHMRC Senior Research Fellowship [APP1019693].
https://doi.org/10.1124/mol.118.115220.
[S] This article has supplemental material available at molpharm.aspetjournals.org.

ABBREVIATIONS: ANOVA, analysis of variance; CiPA, comprehensive in vitro proarrhythmic assay; CL, interpulse time; Fso, fractional state occupancy; Fso_{closed}, state occupancy fraction for the closed state; Fso_{inact}, state occupancy fraction of the inactivated state; Fso_{open}, state occupancy fraction of the open state; ΔIC_{50}, difference in log IC_{50} values; I_{Kr}, rapid component of delayed rectifier current; *Ki*, drug affinity in inactivated state; *Ko*, drug affinity in open state; *KO/I*, relative drug affinity; K_v11.1, voltage-gated potassium channel subtype 11.1; *RO/I*, ratio of the fractional state occupancy of the open state versus the inactivated state, V_h, holding potential; Vr, repolarizing ramp.

observed with different voltage protocols (Potet et al., 2001; Rezazadeh et al., 2004). A recent publication from the comprehensive in vitro proarrhythmia assay (CiPA) initiative (Fermini et al., 2016) acknowledged this issue and noted that it is not possible to predict protocol dependence in advance. Therefore, if a "true" IC_{50} value cannot be reliably determined, then a safety margin is not an effective way of identifying and eliminating risk (Lee et al., 2017).

To address this issue, CiPA has been proposed as a new safety paradigm in understanding torsade de pointes and assessing proarrhythmia risk (Sager et al., 2014). One of the key objectives of CiPA is to use detailed in vitro electrophysiological characterization of drug interaction with $K_v11.1$ to build in silico models to predict arrhythmia risk. One factor that is likely important for this approach, is understanding the state dependence of binding (Lee et al., 2017). It has been shown that for some drugs, the affinity can be as much as 30-fold greater for the inactivated state (*Ki*) relative to the open state (*Ko*) (Suessbrich et al., 1997; Ficker et al., 1998; Perrin et al., 2008a; Wu et al., 2015), whereas other drugs have no apparent state preference (Hill et al., 2014). Furthermore, previous studies have shown that two drugs with opposite state preference (10^4-fold difference in *Ko* vs. *Ki*) but the same IC_{50} values can cause up to a 56-millisecond (~15%) difference in the extent of prolongation of the action potential duration at an IC_{50} dose (Lee et al., 2017). Thus, state preference is an important consideration when determining whether a $K_v11.1$-drug interaction is likely to be proarrhythmic.

In this study, we use both in silico and in vitro approaches to explore the extent to which protocol-dependent differences in $K_v11.1$ drug-binding affinity can be explained by state-dependent drug binding. Additionally, we demonstrate that: 1) measuring potency with a range of voltage protocols that result in different ratios of state occupancy can be used to predict and quantify the state-dependent drug-binding characteristics of a drug; and 2) that the potency of a drug measured using specific individual protocols can be predicted from IC_{50} values measured using other protocols. Importantly, either of these predictions can be made based on simple voltage protocols that are readily amenable to automated, high-throughput patch-clamp platforms. Our work provides a novel method for quantifying the state dependence of $K_v11.1$ drug interaction from simple measures of potency and identifies how state-preferential drug binding is a major determinant of the protocol dependence of IC_{50} measured in preclinical $K_v11.1$ assays.

Materials and Methods

In Silico Modeling. A Markov state model of drug binding to $K_v11.1$ (Fig. 1A; Supplemental Fig. 1) was used to simulate drug block of I_{Kr} (Lee et al., 2016). This model has three closed states (C_0, C_1, C_2), an open-conducting state (O), and an inactivated state (I); and drugs can bind to either the open state (OD) and/or the inactivated state (ID). Transitions between the non–drug-bound states are expressed as rate constants (*kf* for the forward rate and *kb* for the backward rate) and are of the format shown in eqs. 1 and 2:

$$kf = \alpha 0 e^{Z_\alpha \times Vm / \left(\frac{RT}{F}\right)} \quad (1)$$

$$kb = \beta 0 e^{Z_\beta \times Vm / \left(\frac{RT}{F}\right)} \quad (2)$$

where R is the gas constant 8.314, T is the temperature in Kelvin, F is the Faraday constant, Vm is he membrane voltage in millivolts. $\alpha 0$, $Z\beta$, $\beta 0$, and $Z\beta$ values for the model at 37°C are shown in Supplemental Fig. 1. To approximate gating at 22°C (Fig. 9), individual rates (*kf* or *kb*) were scaled for temperature using to Q_{10} values of 2.1, 1.7, 2.5, and 2.6 for activation, deactivation, inactivation, and recovery from inactivation transitions, respectively, as previously reported (Vandenberg et al., 2006).

Drug binding was described as forward and reverse rates for binding to the open state ($kf_{,open}$ and $kb_{,open}$, respectively) and to the inactivated state ($kf_{,inact}$ and $kb_{,inact}$, respectively). Drug association constants for *Ko* and the *Ki* were calculated as the ratio of the forward and reverse binding rates:

$$K = kf/kb \quad (3)$$

The relative drug affinity (KO/I) values for the two states was described as a ratio of the drug association constant of each individual state, as shown in eq. 4. Where $KO/I < 0.5$ indicates a greater relative affinity for the inactivated state, $KO/I > 2$ indicates a greater relative affinity for the open state and $0.5 < KO/I < 2$ indicates drugs that have equal affinity for both states or minimal difference in affinity for either state:

$$KO/I = Ko/Ki. \quad (4)$$

Theoretical Drugs. To examine the effect of state-dependent drug binding on measured potency, we used the same set of 6561 theoretical drugs specified in the study by Lee et al. (2016). This was created through permutations of the two forward and two reverse rates for drug binding in the range of 0.01–100 s^{-1} using half-logarithmic increments (0.01, 0.03, 0.1, 0.3, 1, 3, 10, 30, and 100 s^{-1}) for each drug state transition. For machine-learning training and validation, we used a separate set of 2000 and 1000 theoretical drugs, respectively. In this case, forward and reverse rates of binding were randomly generated in the range of 10^4–10^8 s^{-1} for forward rates, and 0.001–100 s^{-1} for reverse rates. These rates were consistent with previously published in vitro–constrained kinetic data (Windley et al., 2017) and produced IC_{50} values in a physiologic range on the order of 10^{-10} to 10^{-3} M.

Drug-binding simulations were performed using the above described sets of theoretical drugs over a wide range of drug concentrations (10^{-8} to 10^7 M for the initial data set, or 10^{-15} to 0 M for the machine-learning data set). Current was normalized to the control current. For pulsed voltage protocols this was measured as peak current, whereas for nonpulsed protocols was taken as mean current over >100 milliseconds once the current had reached equilibrium. IC_{50} values were calculated from dose-response curves using the Hill equation (eq. 5):

$$y = \frac{1}{1 + 10^{(pIC_{50} - x) \times Hillcoeff}} \quad (5)$$

where y is the normalized peak current amplitude, x is the $\log_{10}$ drug concentration in M, pIC_{50} is the $\log_{10}$ IC_{50} in molar concentration and *Hillcoeff* is the Hill slope of the dose-response curve. Protocol-to-protocol differences in IC_{50} were measured as the $\Delta\log[IC_{50}]$, which is the difference in $\log_{10}$ $[IC_{50}]$ for each protocol. All simulations and analyses were performed using Matlab software (MathWorks, Natick, MA).

Cell Culture. CHO cells stably expressing $K_v11.1$ (cell line PTA-6812) were purchased from the American Type Culture Collection (Manassas, VA). Cells were cultured in Ham's F12 nutrient mix (Thermo Fisher Scientific, Waltham, MA) with added 5% FBS (Sigma-Aldrich, Sydney, NSW, Australia) and maintained at 37°C with 5% CO_2.

Patch-Clamp Electrophysiology. $K_v11.1$ currents were recorded in the whole-cell voltage-clamp configuration at 22°C. The current signal was sampled at 5 kHz and filtered at 1 kHz with an Axopatch 200B amplifier (Molecular Devices, Sunnyvale, CA) interfaced with a Digidata 1440A analog-to-digital converter (Molecular Devices). Series resistance was compensated by at

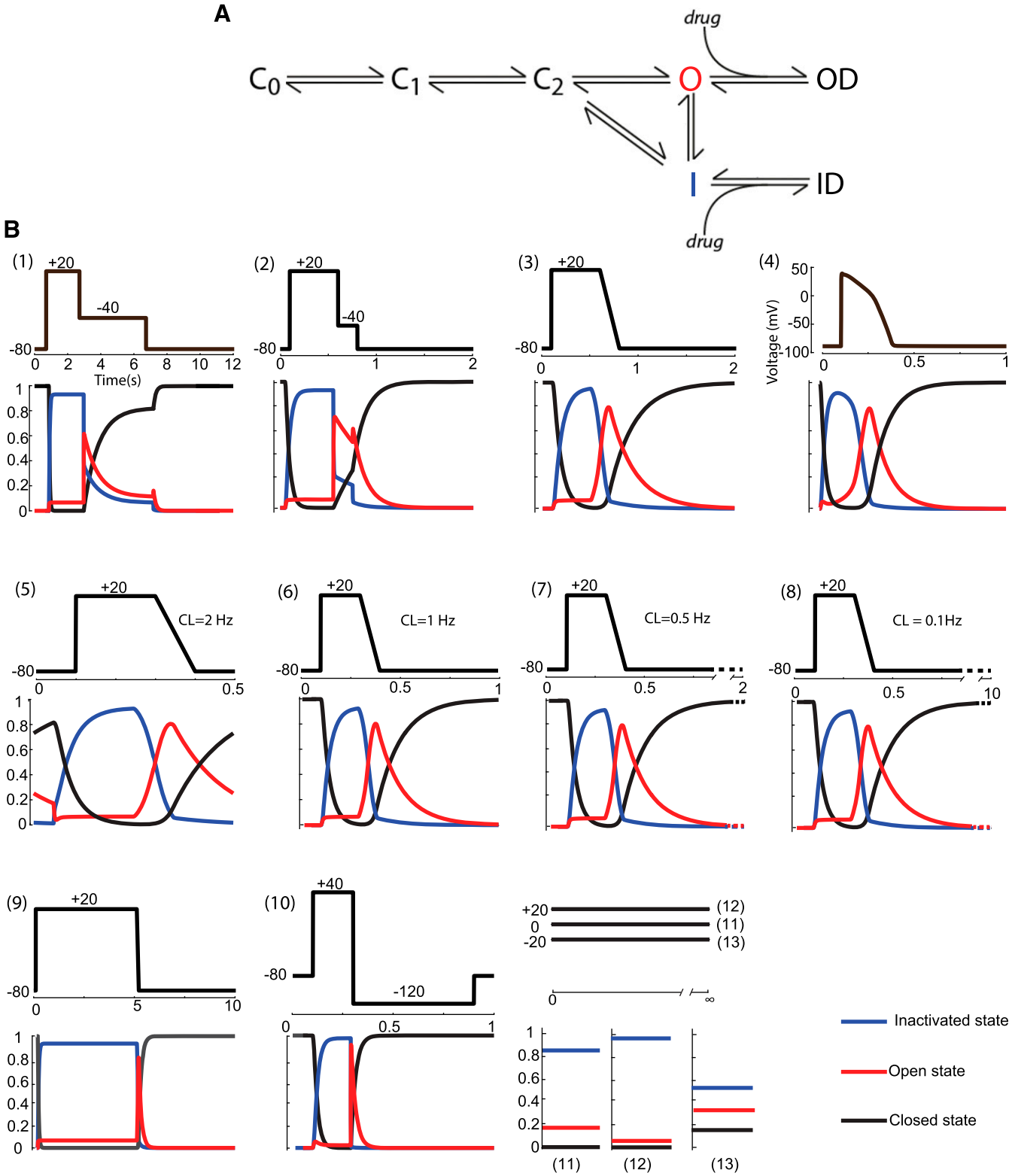

Fig. 1. (A) Markov state model of $K_v11.1$-drug interaction. Parameters describing voltage-dependent $K_v11.1$ gating transitions are presented in Supplemental Fig. 1. (B) Voltage waveforms and their gating state occupancies [open (red), inactivated (blue), closed (black)] for each of the 13 voltage protocols (numbers indicated in parentheses) used. ID, drug bound to the inactivated state; OD, drug bound to the open state.

least 80% in all experiments. External bath solution contained (in mM): 130 NaCl, 5 KCl, 1 $MgCl_2$, 1 $CaCl_2$, 12.5 glucose, and 10 HEPES, adjusted to pH 7.4 with NaOH. Single-use patch pipettes were made from borosilicate glass (Harvard Apparatus, Holliston, MA) and pulled using a vertical two-stage puller (PP-830; Narishige, Tokyo, Japan) with resistance of 2–4 MΩ. Pippettes were filled with an internal solution containing (in mM): 120 potassium gluconate, 20 KCl, 1.5 Mg_2ATP, 5 EGTA, and 10 HEPES, adjusted to pH 7.4 with KOH. Data were corrected for a calculated liquid junction potential of −15 mV. Data

were acquired with pCLAMP 10 acquisition software (Molecular Devices). Leak currents were subtracted off-line and data analysis was performed using Clampfit (Molecular Devices), Prism (version 7; GraphPad Software, San Diego, CA), and Matlab (MathWorks).

Pharmacology. Verapamil, terfenadine, cisapride, and clozapine were purchased from Sigma-Aldrich and dissolved in DMSO. The maximum final concentration of DMSO in the recording solution was less than 0.01% (v/v), which is well below the 0.1% (v/v) shown to have no effect on K_v11.1 activity (Walker et al., 1999). Drugs were delivered via a Dynaflow Resolve microfluidic device (Cellectricon, Mölndal, Sweden), allowing the delivery of discrete solutions of various drug concentrations under laminar flow with a solution exchange time of less than 30 milliseconds. Current amplitudes were measured when steady state had been achieved. Five drug concentrations were used to construct a Hill curve and calculate an IC_{50} value for verapamil, cisapride, and clozapine. Three concentrations were used for terfenadine as drug binding has very slow kinetics, and we wished to avoid significant current rundown while allowing sufficient time for drug binding to reach steady state.

Voltage Protocols. We studied 13 voltage protocols that reflected the range of commonly used published voltage protocols as well as incorporating variations in cycle length, which allowed sampling of the K_v11.1 at different amplitudes and durations of state occupancy. Voltage waveforms and their corresponding state occupancies for the open (red), inactivated (blue), and closed (black) states are shown in Fig. 1B. All protocols had a holding potential (V_h) of −80 mV, unless otherwise stated. Protocol 1 was a two-step protocol with an initial step (V_1) to +20 mV for 2 seconds followed by a −40 mV step (V_2) for 4 seconds and a total interpulse time (CL) of 12 seconds. (Milnes et al., 2010). Protocol 2 was also a two-step protocol with V_1 = +20 mV for 500 milliseconds, V_2 = −50 mV for 200 milliseconds, and CL = 2 seconds (Yao et al., 2005). Protocol 3 was a step-ramp protocol with a V_1 = +20 mV for 500 milliseconds, followed by a repolarizing ramp (V_r) of −0.5 V/s, CL = 2 seconds (Yao et al., 2005). Protocol 4 was the voltage waveform of an O'Hara Rudy action potential (O'Hara et al., 2011). Protocols 5–8 consisted of a step ramp with V_1 = +20 mV for 200 milliseconds, V_r = 1 V/s, and CL of 500 milliseconds, and 1, 2, and 10 seconds, respectively. Protocol 9 was a step-ramp protocol with a long V_1 step of 5 seconds at +20 mV, followed by V_r = 1 V/s and CL = 10 seconds. Protocol 10 was a two-step protocol with V_1 = +40 mV for 200 milliseconds, V_2 = −120 mV for 600 milliseconds, and CL = 1 seconds, resulting in a negative hook-tail current (Perrin et al., 2008a). Finally, protocols 11–13 were performed with direct application of the drug during voltage holding at V_h = 0 (Hill et al., 2014), +20, and −20 mV, respectively, and CL = ∞. For in vitro experiments and in silico machine-learning algorithms, a subset of six of the above protocols were used; this included protocols 1, 8, 10, 11, 12, and 13. Specific details of individual protocols as well as evoked K_v11.1 currents from in silico and in vitro experiments are shown in Supplemental Figs. 2–14.

To quantify the state occupancy fraction of open state (Fso_{open}) and inactivated state (Fso_{inact}) for each voltage protocol, a time integral of state occupancy was calculated for each state as follows:

$$\mathrm{Fso} = \left(\int_0^{CL} State\ Occupancy \right) \Big/ CL \tag{6}$$

Where *State Occupancy* represents the state occupancy for each of the three states (Open = O, Inactivated = I, or Closed = C_1 + C_2 + C_3) defined in the Markov model above in the section "In Silico Modeling," and CL is the total interpulse time, as stated above. The ratio of the fractional state occupancy of the open state versus the inactivated state (RO/I) for each voltage protocol was therefore defined in eq. 7:

$$R_{O/I} = \frac{\mathrm{Fso}_{open}}{\mathrm{Fso}_{inact}}. \tag{7}$$

Machine Learning. A subset of six voltage protocols was chosen that maximized the differences in state occupancy for the three states and demonstrated the largest variation in in silico IC_{50} measurements. This subset was used to simulate and measure IC_{50} values using the randomly generated 2000 training and 1000 validation theoretical drug sets. These sets of IC_{50} values were then used to train and validate machine-learning algorithms to predict drug-binding characteristics including state-preference and protocol-dependent affinity. All machine-learning prediction algorithms were generated and validated using the Matlab Neural Network fitting application (MathWorks). Training data sets were normalized (z-score) to have a mean of 0 and a S.D. of 1. Validation data sets were z-score transformed using the mean and S.D. of their respective training set. Neural networks were constructed using between 10 and 100 neurons within one hidden layer. The neural network which best fitted the training data set was then tested for overfitting using the corresponding validation data set.

Statistical Methods. Analysis of variance (ANOVA) was used for statistical analysis between normally distributed data for multiple

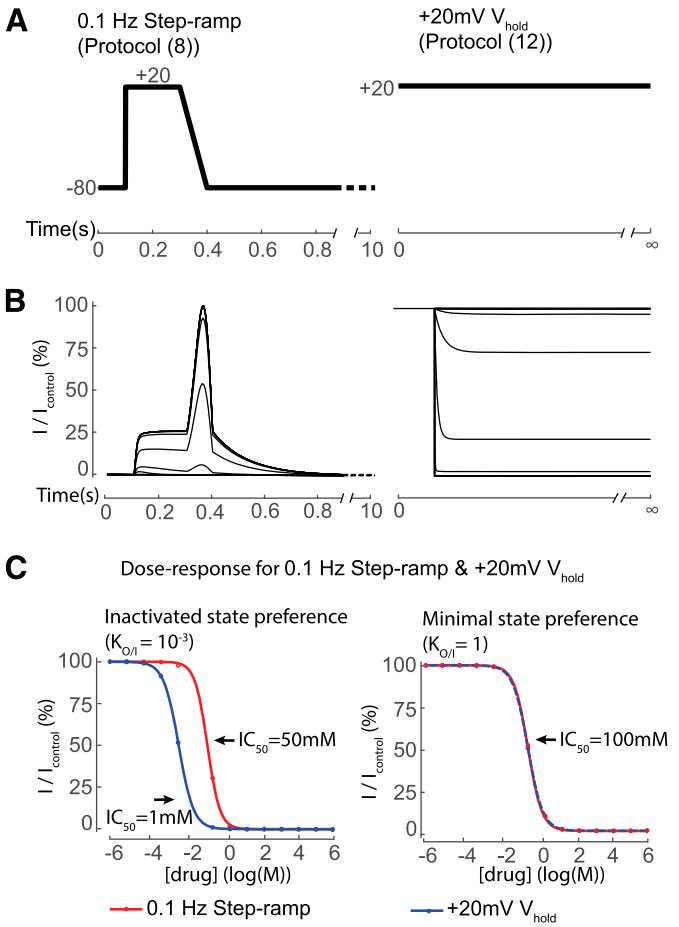

Fig. 2. (A) Voltage waveforms for the 0.1-Hz step-ramp protocol 8 and the nonpulsed +20-mV V_h protocol 12. (B) Examples of in silico simulated K_v11.1 currents evoked when voltage clamped using voltage protocols 8 (left) and 12 (right), in the presence of increasing concentrations of drug (10^{-6} to 10^{6} M is shown). (C) Dose-response curves derived from normalized peak current amplitude shown in (B). The left-side graph demonstrates a 50-fold difference in measured IC_{50} between the two protocols for a drug that preferentially binds to the inactivated state ($KO/I = 10^{-3}$). In comparison, the right-side graph shows a drug that has no state preference (KO/I = 1) has no difference in measured IC_{50} values between the two protocols.

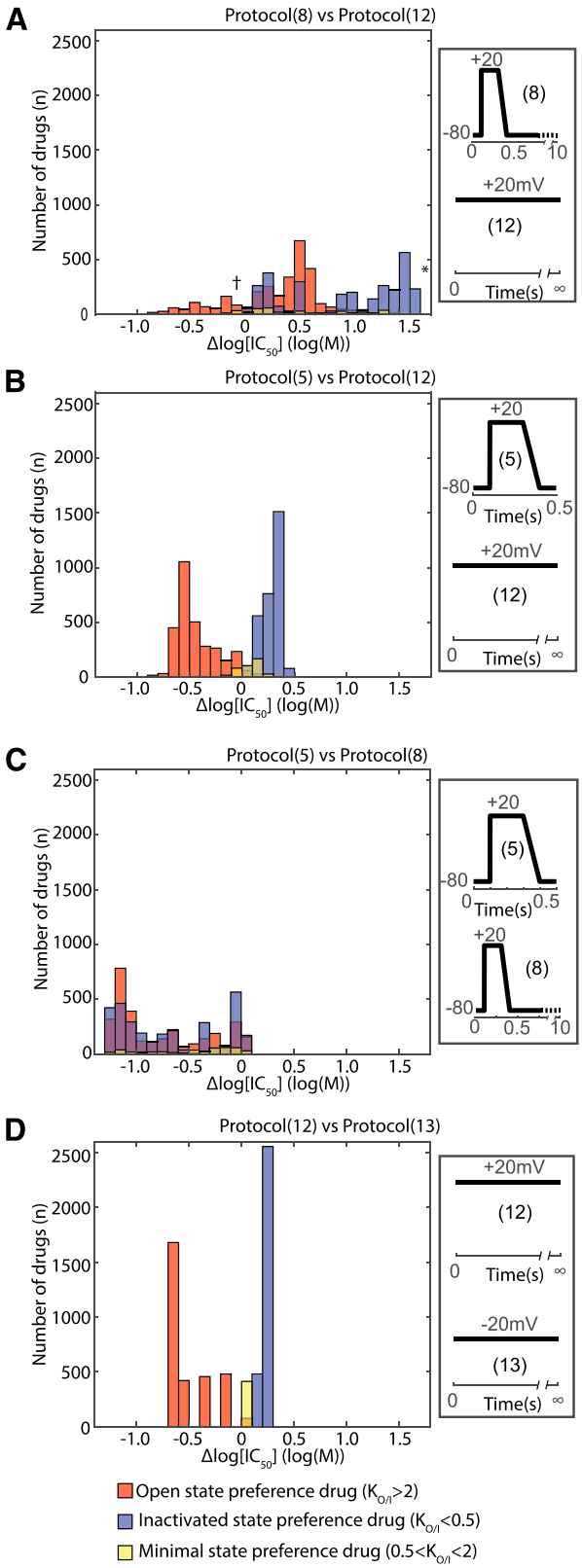

Fig. 3. Differences in IC_{50} values between two protocols for 6561 theoretical drugs. Drugs are grouped by preferential binding to the open state ($KO/I > 1$, red), inactivated state ($KO/I < 1$, blue), and minimal state ($0.5 < KO/I < 2$, yellow) preference. (A) Shows a wider landscape of comparison between protocol 8 and protocol 12. The inactivated state-preference drug and non–state-preference drug examples are marked with * and †, respectively. The difference in IC_{50}, measured as the difference in $\log_{10}[IC_{50}]$ ($\Delta\log[IC_{50}]$) between these two protocols spans over a wide range with some grouping with respect to drug state preference. (B) Comparison between IC_{50} values from protocol 5 and protocol 12, showing more distinct grouping with respect to state preference. (C) Comparison between IC_{50} values from protocol 5 and protocol 8: no obvious grouping is seen with respect to drug state preference due to the very similar waveform of the two voltage protocols. But up to a 20-fold variation in IC_{50} is still observed, indicating mechanisms other than state preference can influence drug affinity to K_v11.1. (D) Comparison between IC_{50} values from protocol 12 and protocol 13: very distinct grouping with respect to drug state preference is seen over a smaller range. The right side panels (A–D) show the waveforms of the two voltage protocols being compared for their respective histogram.

groups. P values of <0.05 were considered significant. Statistical analyses were performed in Matlab (MathWorks).

Results

In Silico Variations in Measured Drug Affinity to K_v11.1. To test the influence of state preferential drug binding on variation in measured K_v11.1 affinity, we simulated block of K_v11.1 using two voltage protocols that have been used in previously published studies (Milnes et al., 2010; Hill et al., 2014). We simulated dose-response curves for an inactivated state–preference drug with a 1000-fold higher affinity for the inactivated state versus open state ($KO/I = 10^{-3}$). Example simulated currents in response to increasing concentrations of the inactivated state–preference drug for the two protocols are shown in Fig. 2B. For each protocol, a Hill curve was fit to the simulated data to derive an IC_{50} value for channel block. The inactivated state–preference drug had a 50-fold higher affinity for K_v11.1 when measured using the +20-mV V_h protocol 12 compared with the 0.1-Hz step-ramp protocol 8 (Fig. 2C, left panel) (IC_{50} = 1 and 50 mM, respectively). As a comparison, we also simulated block using a non–state-preference drug, which showed no difference in K_v11.1 affinity between the two protocols (IC_{50} = 100 mM) (Fig. 2C, right panel).

To probe the protocol dependence of measured K_v11.1 affinity in more detail, we extended our study to a panel of 6561 theoretical drugs with varying state preferences and a larger array of 13 voltage protocols (Fig. 1B; Supplemental Figs. 2–14). For each combination of drug and protocol, a dose-response curve was simulated (as shown in Fig. 2B) and an IC_{50} value derived through fit of the Hill equation. For each drug, we then calculated the difference in log IC_{50} values (ΔIC_{50}) between pairs of protocols and grouped them with respect to state preference (Fig. 2B: inactivated state preference $KO/I < 0.5$ are colored blue; open state preference $KO/I > 2$ are colored red; and minimal-state preference $0.5 < KO/I < 2$ are colored yellow) (Fig. 3). This pairwise analysis of protocols gave a total of 78 comparisons.

We first examined the distribution of ΔIC_{50} values measured using the same two protocols shown in Fig. 2 (protocols 8 and 12; Fig. 3A). We observed a wide range of ΔIC_{50} values, from −0.9 to 1.7 which equates to a difference in IC_{50} for protocol 8 versus protocol 12 of 8-fold less or 50-fold higher. Overall, drugs tended to be grouped by state preference. Although all drugs tended to have a higher affinity when measured with protocol 12, this effect was most pronounced for inactivated state–preference drugs. For reference, the inactivated state–preference drug example from Fig. 2 is marked as with a * symbol, and the non–state-preference drug is marked with a † symbol. Other

protocol comparisons gave much clearer separation of drugs according to their state preference. A pairwise comparison of protocols 5 and 12 (Fig. 3B) resulted in a clear bimodal separation of drugs based on open/inactivated state preference, with inactivated state–preference drugs displaying a higher affinity and open-state–preference drugs having a lower affinity for protocol 12 relative to protocol 5. Consistent with our previous observations, non–state-preference drugs had minimal or no difference in measured IC_{50} values between protocols. It is important to note that subtle differences in the protocols being compared can significantly affect the observed distributions for ΔIC_{50}. For example, in Fig. 3, A and B, protocol 12 is compared against protocols 8 and 5, respectively. The only difference between protocols 5 and 8 is the CL (500 vs. 10,000 milliseconds), yet the observed distributions (compare Fig. 3, A and B) are clearly different, highlighting that it is not solely the "test pulse" component of the protocol that is important in defining the measured potency. Conversely, when protocols 5 and 8 are compared against each other (Fig. 3C), there is no observable clustering of drugs based on their state preference. However, the fact that there were still observable differences in ΔIC_{50} values between two protocols for different drugs (maximum ΔIC_{50}, −1.3 or +0.1) suggests that state preference of binding is not the only factor that influences protocol-dependent affinity.

Finally, we examined an example of a pairwise comparison between nonpulse protocols. A comparison of ΔIC_{50} for protocols 12 and 13—static V_h values of +20 and −20 mV respectively—is shown in Fig. 3D. We observed a distinct grouping of drugs based on state preference, albeit over a smaller range of ΔIC_{50} values, from −0.7 to 0.2 difference between the two protocols. In this case, inactivated state–preference drugs had a higher affinity for protocol 12 and open state–preference drugs for protocol 13. It is notable that these two protocols show the greatest separation of drugs based on state preference as they are pure equilibrium measures, meaning that there is no cycling of state occupancy among the open, inactivated, and closed states during the protocol, and consequently there is no influence from drug-binding kinetics.

Given this varied separation of drugs with different pairs of protocols, we next investigated which pairwise comparison gave the greatest ΔIC_{50} across all our drugs. To do this, we took the maximum ΔIC_{50} from each pairwise comparison for each drug (Fig. 4). This demonstrated that the maximum ΔIC_{50} was most often observed for comparisons between protocols 8 and 12, as well as between protocols 8 and 13 (Fig. 4A) (for voltage waveforms, refer to Fig. 1B, protocols 8, 12, and 13). More specifically, we observed that open state–preference drugs tended to have a maximum ΔIC_{50} between protocols 8 and 13 (for voltage waveforms, refer to Fig. 1B, protocols 8 and 13), while inactivated state–preference and non–state-preference drugs tended to have a maximum ΔIC_{50} value between protocols 8 and 12 (Fig. 4B) (for voltage waveforms, refer to Fig. 1B, protocols 8 and 12). This supports the idea that individual voltage protocols sample distinct gating state "space" and hence differentially interact with state preferential drug binding to determine these shifts in IC_{50}.

Voltage Protocol Dependence of State Occupancy. To better understand the mechanism behind these observations, we next examined how the state occupancy of the $K_v11.1$ channel varies with different voltage protocols. We examined the underlying $K_v11.1$ state occupancy during the three most prominent voltage protocols from Fig. 4. Shown in Fig. 5A are the voltage waveforms for the 0.1-Hz step-ramp protocol (protocol 8) and the two nonpulsed V_h protocols at +20 and −20 mV (protocols 12 and 13, respectively). The respective time-varying state occupancy for the open (red), closed (black), and inactivated (blue) states of the channel during each of these protocols is shown in Fig. 5B. To compare the relative occupancy over time, for each protocol we calculated the state occupancy time integral for each state expressed as a fraction of the total time integral [i.e., Fso_{open}, Fso_{inact}, and state occupancy fraction for the closed state (Fso_{closed})] (Fig. 5C) (eq. 6) (*Materials and Methods*).

The relative occupancy of the open versus inactivated states (i.e., *RO/I*) for the different protocols is shown as a number above each protocol in Fig. 5C. All the protocols we tested had

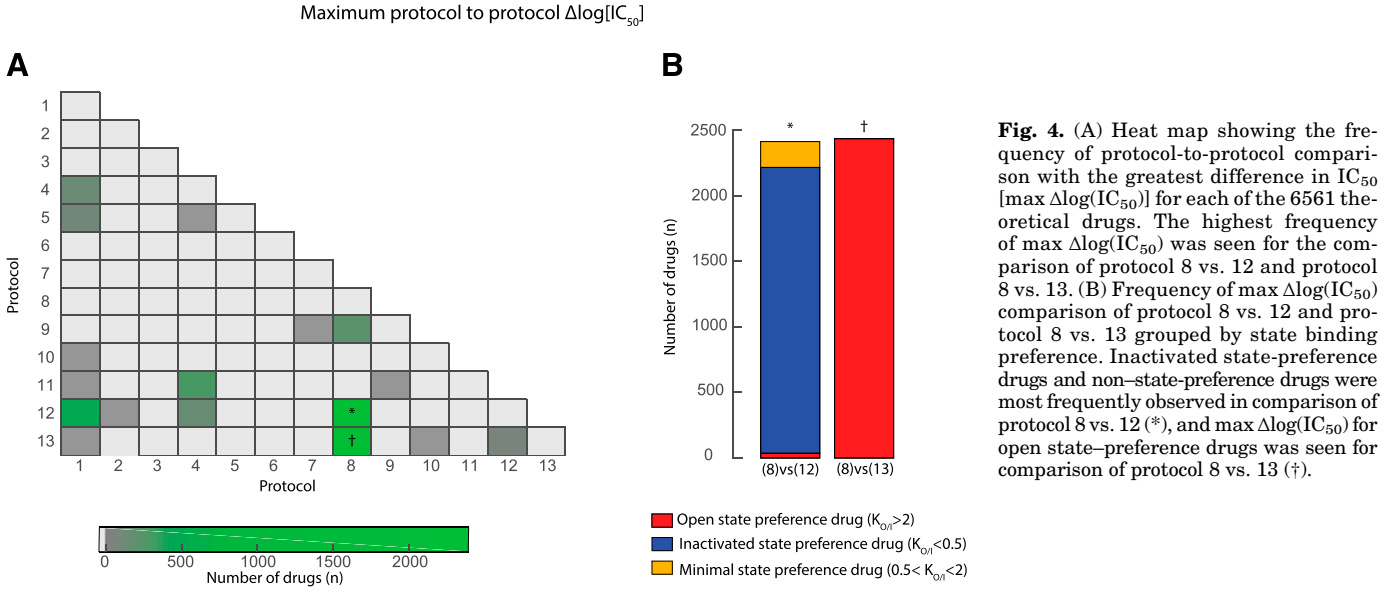

Fig. 4. (A) Heat map showing the frequency of protocol-to-protocol comparison with the greatest difference in IC_{50} [max $\Delta\log(IC_{50})$] for each of the 6561 theoretical drugs. The highest frequency of max $\Delta\log(IC_{50})$ was seen for the comparison of protocol 8 vs. 12 and protocol 8 vs. 13. (B) Frequency of max $\Delta\log(IC_{50})$ comparison of protocol 8 vs. 12 and protocol 8 vs. 13 grouped by state binding preference. Inactivated state-preference drugs and non–state-preference drugs were most frequently observed in comparison of protocol 8 vs. 12 (*), and max $\Delta\log(IC_{50})$ for open state–preference drugs was seen for comparison of protocol 8 vs. 13 (†).

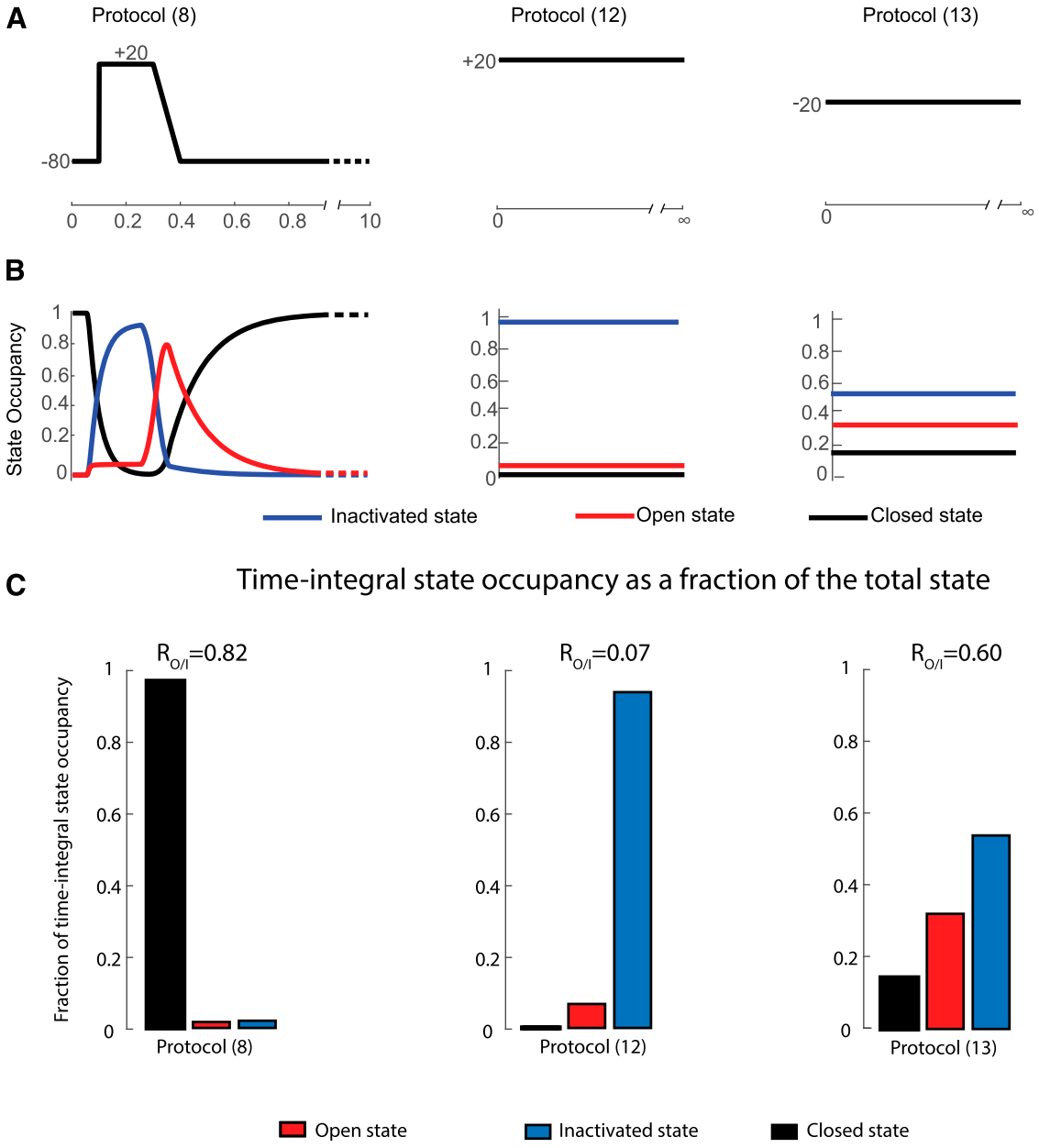

Fig. 5. (A) Voltage protocols for the subset of 3 of the 13 protocols (numbers in parentheses) with the greatest frequency of max $\Delta\log(IC_{50})$ from Fig. 4; used for in silico machine-learning training and validation. (B) State occupancies for the open (red), inactivated (blue), and closed states (black) (shown as a fraction of total state occupancy) for each of the three protocols depicted in (A). (A and B) are taken from Fig. 1. (C) Relative Fso for the open (red), inactivated (blue), and closed (black) states, expressed as a time-integral fraction or area under the curve of the state occupancies shown in (B). Relative state-occupancy (RO/I) of each protocol representing the ratio of Fso_{open} to Fso_{inact} is shown above each column graph.

a $RO/I < 1$, indicating that there was a greater probability of channels spending time in the inactivated state than the open state. For the two nonpulsed protocols (protocols 12 and 13), RO/I decreased with increasing voltage (0.6 and 0.07 for −20 and +20 mV, respectively), consistent with the known voltage-dependent inactivation behavior of K_v11.1 The pulsed protocol (protocol 8) had a close to equal time spent in the open and inactivated states with an $RO/I = 0.82$. However, the pulsed protocol (protocol 8) dwelt predominantly in the closed state (Fso_{closed}, 96.3%) in contrast to the nonpulsed protocols (Fso_{closed}, 0.03% and 14.2% for protocols 12 and 13, respectively). In keeping with this, a lower occupancy of the open and inactivated versus closed states was evident for the pulsed protocol (protocol 8) compared with the nonpulsed protocols 12 and 13 (Fig. 5C).

These data suggest that protocol 12, having the lowest RO/I, will be the most sensitive to inactivated state–preference drugs, whereas protocol 8 will be almost equal in sensitivity to open state–preference and inactivated state–preference drugs. Moreover, the observation in Fig. 4 that inactivated state–preference drugs were most likely to have a maximum difference in affinity between protocols 8 and 12 can be attributed to the large difference in Fso_{inact}. Similarly, the maximum difference in affinity for open state–preference drugs is seen between protocols 8 and 13 due to the large difference in Fso_{open} values between these protocols.

In Silico Prediction of State Preferential Drug-Binding Characteristics. Our observations so far suggest that the state-dependent binding properties of the drug and the gating state occupancy of the channel (as a function of the voltage protocol) interact in a predictable way to determine the differences in measured potency between protocols. To further test this hypothesis, we sought to demonstrate the corollary of this (i.e., use measured differences in IC_{50} to predict the state preference of a drug. To do this, we measured IC_{50} values for 2000 in silico drugs using protocols 8, 12, and 13 (for voltage waveforms, refer to Fig. 1B, protocols 8, 12, and 13) and from these created a set of three pairwise comparisons of ΔIC_{50}. This set of pairwise comparisons was then used to train a neural network. A second set of 1000 different drugs was then used to test the accuracy of our predictions (Fig. 6). Overall, the model performed extremely well, with a Pearson's correlation coefficient between predicted and true state preference (KO/I) of $R = 0.930$.

We then sought to test whether the same three pairwise comparisons of ΔIC_{50} could be used to predict IC_{50} values for other voltage protocols. We were able to predict IC_{50} values in all cases (protocols 11, 1, and 10) (for voltage waveforms, refer to Fig. 1B, protocols 11, 1, and 10) with a high degree of accuracy (Fig. 7). In silico predictions (shown in black) for protocols 1, 10, and 11 had a correlation coefficients of $R = 0.984$, $R = 0.988$, and $R = 0.999$, respectively.

In Vitro Measurement of Protocol Dependence of IC_{50}. We next tested whether drugs with varying state preference also showed different measured potencies in manual patch-clamp electrophysiology assays, depending on the voltage protocol used. Typical $K_v1.1$ current traces recorded using six of the protocols examined in silico (1, 8, 10, 11, 12, and 13) for voltage waveforms, refer to Fig. 1B, protocols 1, 8, 10, 11, 12, and 13) in response to increasing (cisapride) are shown in Fig. 8. To highlight the differences in measured potency among the protocols, the 60 nM dose of cisapride is highlighted in red in Fig. 8 for each case. For the short pulse protocols (8 and 10), 60 nM cisapride blocked measured current by ~25%. In comparison, the same concentration caused a 75%–80% reduction in current amplitude when measured using the long-pulse protocol (protocol 1) or the non–pulse protocols 11, 12, and 13.

The same set of in vitro experiments were also carried out for three other drugs (clozapine, verapamil, and terfenadine), dose-response curves constructed for each of the six protocols (Fig. 9, A–D, left-side panels), and IC_{50} values derived from fits of the Hill equation (Fig. 9, A–D, right-side panels) (for voltage waveforms, refer to Fig. 1B, protocols 1, 8, 10, 11, 12, and 13). Maximums of 2.79-fold, 8.32-fold, 1.93-fold, and 3.09-fold ΔIC_{50} values, respectively, were measured between protocols for verapamil, cisapride, clozapine, and terfenadine. Overall, significant differences between the IC_{50} values measured using the six protocols were observed for verapamil, cisapride, and terfenadine ($P = 0.0297$, 0.0005, and 0.001, respectively; ANOVA), but not for clozapine ($P = 0.3406$). This result suggests that verapamil, cisapride, and terfenadine may have state preferential binding properties. Furthermore, verapamil, and cisapride demonstrated a higher affinity when measured with protocol 12 compared with protocol 8 (1.77-fold and 5.96-fold ΔIC_{50}, respectively), consistent with our in silico model observations for inactivated state–preference drugs (Fig. 2; Fig. 3A).

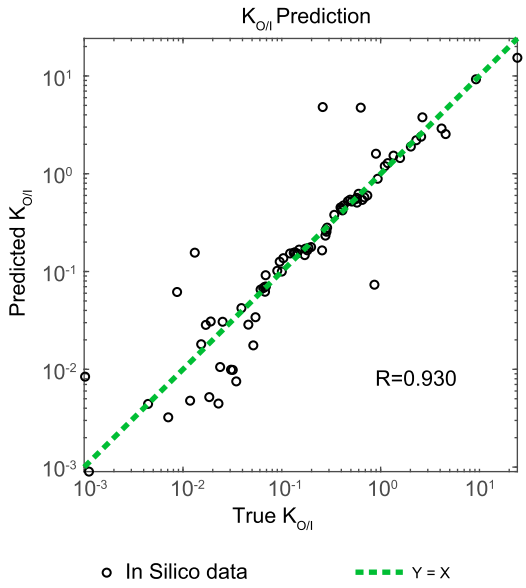

Fig. 6. In silico neural network algorithm was trained using IC_{50} values from protocols 8, 12, and 13 to predict the KO/I for that drug. A separate in silico data set was used to independently validate the prediction algorithm (shown in black). An identity line (Y = X) is shown as the dashed green line. The accuracy of algorithm predictions is represented as the correlation coefficient R to the identity line.

To understand these observed differences in IC_{50} values, we again considered the channel state occupancy during the individual voltage protocols. For consistency between in vitro experiments and in silico state occupancy calculations, the state occupancies in Fig. 9E were calculated for 22°C by scaling the transition rates in the Markov model (Fig. 1) for temperature (see *Materials and Methods*). For cisapride, there is a correlation between measured potency and Fso_{inact} (i.e., lower IC_{50} values were measured for protocols with greater Fso_{inact} values (protocols 11, 12, and 13) (for voltage waveforms, refer to Fig. 1B, protocols 11, 12, and 13), and the highest IC_{50} values were measured for protocols with the lowest Fso_{inact} values (protocol 8), consistent with preferential binding to the inactivated state. In addition to this, among the pulsed protocols, block by cisapride is less potent when measured with the short-pulsed protocols 8 and 10 (for voltage waveforms, refer to Fig. 1B, protocols 8 and 10), which have lower Fso_{open} and Fso_{inact} values compared with the long-pulsed protocol 1 (for voltage waveform, refer to Fig. 1B, protocol 1) (Fig. 9E). This suggests that there is a requirement for a longer channel opening time in order for the drug-bound states (either open or inactive) to reach their true equilibrium. Overall, a similar pattern was observed for verapamil, though to a lesser degree (Fig. 9A).

For terfenadine, although there are significant differences in the potency of block measured among protocols, the correlation between IC_{50} and Fso_{inact} is not apparent. In particular, the relationship is disrupted by the downward shift in IC_{50} measured using protocols 8 and 10 (e.g., compared with cisapride) (for voltage waveforms, refer to Fig. 1B, protocols 8 and 10). We note that these protocols have a greater proportion of Fso_{closed}, suggesting that drug remaining bound to the closed state or drug trapping may be a modulating factor in the measured IC_{50} value for terfenadine. Finally, for clozapine, the potency of the block was the same

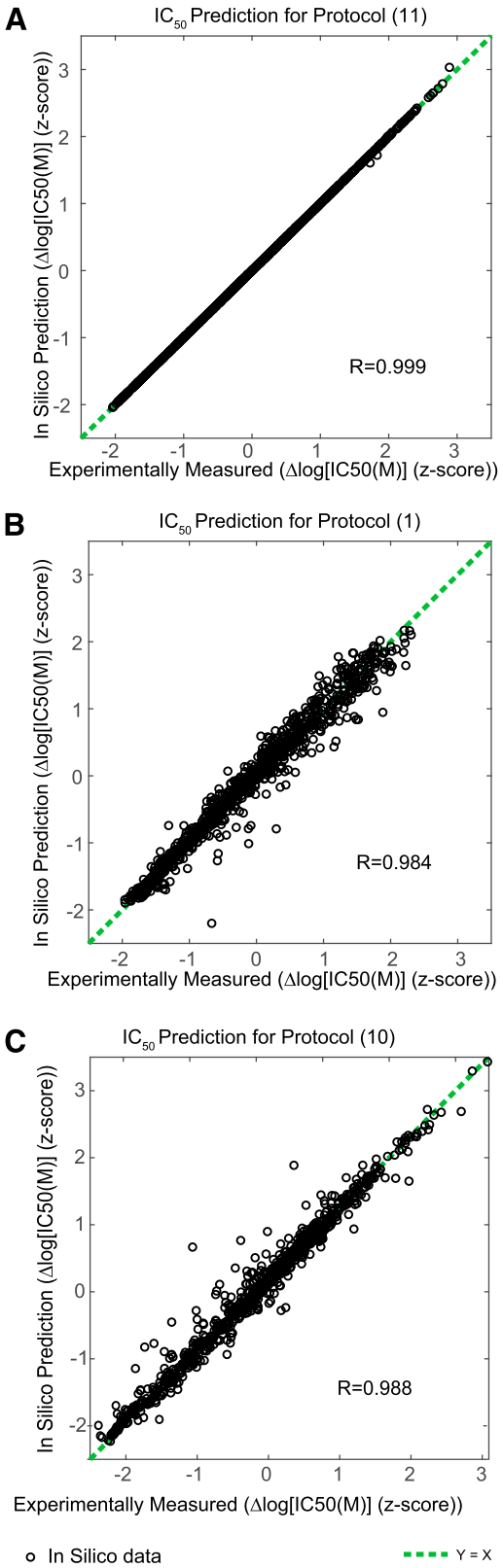

Fig. 7. In silico neural network algorithms were trained using IC_{50} values from protocols 8, 12, and 13 to predict IC_{50} values for other voltage protocols. An independent data set using in silico data (black) was then used to validate the algorithm. Validation performance for each algorithm is shown in each of the three panels showing predictions for the IC_{50} value for protocol 11 (A), the IC_{50} value for protocol 1 (B), and the IC_{50} value for protocol 10 (C). An identity line (Y = X) is shown as a dashed green line. The accuracy of algorithm predictions is represented as the correlation coefficient R to the identity line for each prediction algorithm. The predicted and experimentally measured IC_{50} values are shown as the z-score–transformed $\Delta\log[IC_{50}]$.

regardless of the state occupancy of the voltage protocol used (Fig. 9C).

In Silico Prediction of In Vitro Drug-Binding Characteristics. Since there appears to be a qualitative agreement between state occupancy and measured potency for most of the drugs tested, we next sought to use our in silico trained prediction algorithm (Fig. 6) to predict the state preference (KO/I) of the four drugs using the in vitro measurements of IC_{50} from protocols 8, 12, and 13 (for voltage waveforms, refer to Fig. 1B, protocols 8, 12, and 13). KO/I predictions for verapamil, cisapride, clozapine, and terfenadine are shown in Table 1.

Similarly, we used the algorithms from Fig. 7 to predict the measured IC_{50} values of other in vitro voltage protocols 1, 10, and 11 (for voltage waveforms, refer to Fig. 1B, protocols 1, 10, and 11). Predictions for our four in vitro drugs (verapamil, cisapride, clozapine, and terfenadine) are shown in Fig. 10 in red. To put these in vitro predictions in context, we added the predictions of our 1000 theoretical in silico drugs from Fig. 7 in gray. A similar prediction accuracy was achieved for the four in vitro drug predictions (shown in red) as for the in silico drug predictions. Notably, in vitro IC_{50} prediction algorithms were better for the nonpulse protocol (protocol 11) (Fig. 10A) and the long-pulse protocol (protocol 1) (Fig. 10B), compared with the short-pulse protocol (protocol 10) (Fig. 10C). Overall, our accuracy of in vitro IC_{50} prediction using our in silico prediction algorithm, was within one logarithmic unit of the measured in vitro IC_{50} in all but one case. Details of in vitro measured and in silico predicted IC_{50} values, respective Hill coefficients, as well as KO/I values are shown in Supplemental Table 1.

Discussion

In this study, we have shown that state-dependent drug binding to K_v11.1 channels is a significant factor in determining the range of IC_{50} values measured for individual compounds using different voltage protocols. Furthermore, these differences occur in a predictable manner as a function of the state occupancy of the channel. As a result, both the state preference of a drug as well as its potency measured using other voltage protocols can be inferred from simple equilibrium measures of block.

Factors Contributing to Protocol-Dependent Potency of Block. The variability in potency of K_v11.1 block measured using different voltage protocols has been reported in several studies (Kirsch et al., 2004; Yao et al., 2005; Milnes et al., 2010). For example, the IC_{50} for cisapride varies over a 60-fold range, depending on the protocol used (Potet et al., 2001; Rezazadeh et al., 2004). Our data demonstrate that the synergy of the state preference in drug binding as well as voltage protocol–dependent state occupancy results in such observed variations in affinity. Therefore, drugs that preferentially bind to a specific gating state will have a higher measured affinity for K_v11.1 when using a voltage protocol that favors that gating state, and vice versa. In contrast, for drugs that have no state preference there is no dependence of

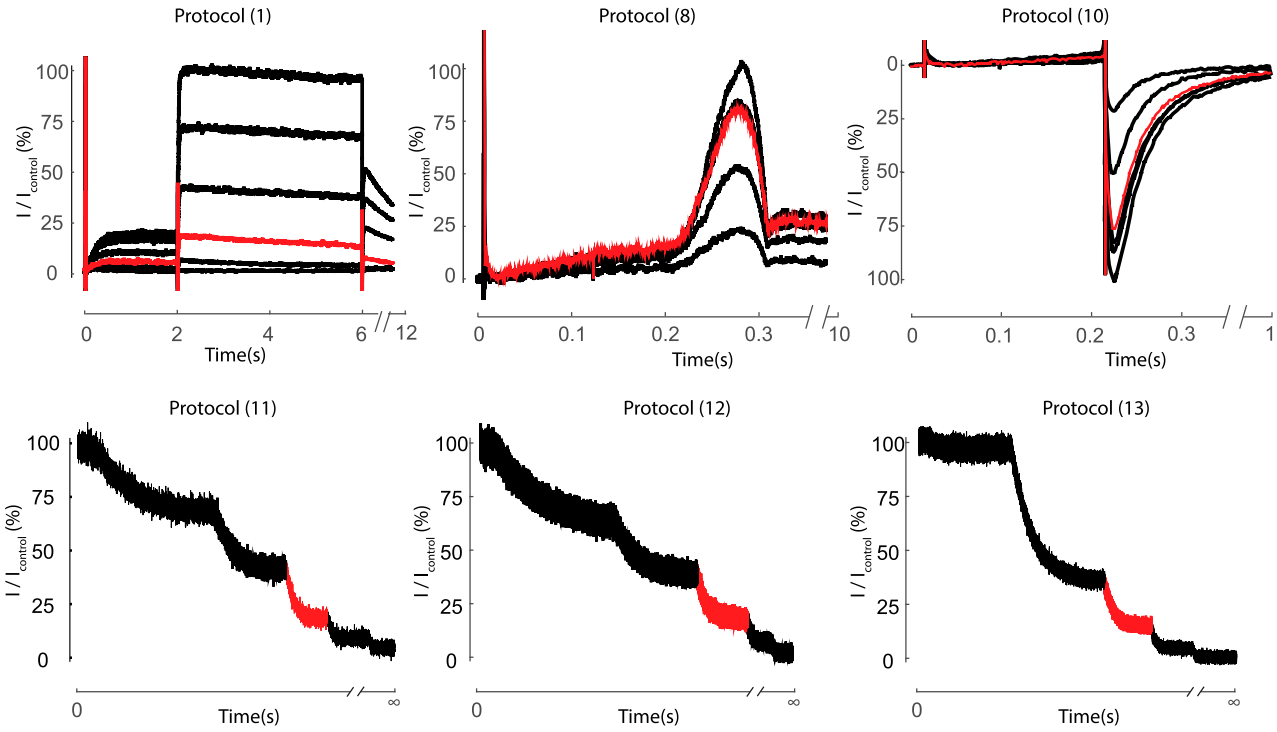

Fig. 8. In vitro experimental data of evoked I_{Kr} currents for six voltage protocols using CHO cells stably expressing $K_v11.1$. $K_v11.1$ currents were measured while cells were perfused with a bath solution in 0, 10, 20, 60, 200, and 600 nM cisapride. Highlighted in red is the I_{Kr} current perfused with 60 nM cisapride for each of the six protocols, demonstrating protocol-to-protocol variation in the degree of $K_v11.1$ block with the same dose of drug concentration.

the measured IC_{50} on the voltage protocol used. However, the data in Fig. 3 demonstrates that variations in IC_{50} values can also occur regardless of state preference, suggesting that the kinetics of drug binding can also have an impact on measured potency. Drugs that block $K_v11.1$ require channel opening to gain access to their binding site in the inner cavity of the channel pore (Ficker et al., 1998; Walker et al., 1999). Therefore, drugs with slow binding kinetics will have a relatively lower affinity when measured using protocols where occupancy of the open/inactivated states is short (relative to the on rate for drug binding) and have a relatively higher apparent affinity when measured using voltage protocols with long depolarization steps or nonpulsed protocols that promote prolonged occupancy of the open and inactivated states. In our in vitro data, this phenomenon is particularly evident for cisapride (Fig. 9B), which has a lower potency when measured using short-pulse protocols (protocols 8 and 10) (for voltage waveforms, refer to Fig. 1B, protocols 8 and 10) where channel open times are on the order of hundreds of milliseconds. This is consistent with previous publications measuring the time-course of block of $K_v11.1$ by cisapride with time constants of ~20 seconds (Windley et al., 2016, 2017).

Another factor that may modify the measured potency of a drug in a protocol-dependent manner is trapping, whereby upon closing of the channel in response to membrane repolarization, a drug is unable to dissociate from the channel cavity (Mitcheson et al., 2000). As a result, accumulation of block can occur for trapped drugs over successive sweeps of a protocol with a high proportion of Fso_{closed} (Li et al., 2017; Windley et al., 2017). Conversely, nontrapped drugs dissociate during the closed intervals, resulting in a lower measured potency. The differences in our in vitro IC_{50} values for terfenadine and cisapride are consistent with this. The potency of block for cisapride, a nontrapped drug (Li et al., 2017; Windley et al., 2017) measured using protocols 8 and 10 (with Fso_{closed} of 95% and 78%, respectively) (for voltage waveforms, refer to Fig. 1B, protocols 8 and 10) is less than when measured using all other protocols that have lower Fso_{closed}. Conversely, for terfenadine, a trapped drug (Kamiya et al., 2008; Windley et al., 2017), the potency measured with protocols 8 and 10 (for voltage waveforms, refer to Fig. 1B, protocols 8 and 10) is increased relative to the other protocols, consistent with the accumulation of block in the closed state. This ability to identify truly trapped drugs, as opposed to those such as cisapride that display "virtual trapping" as a result of slow unbinding kinetics (Windley et al., 2017), is important since it has been suggested that "true" trapping may confer an additional arrhythmia risk (Di Veroli et al., 2014).

We also noted some variation in the Hill coefficients measured across the various in vitro protocols (see Supplemental Table 1). Although most of the coefficients were close to 1, consistent with previously published reports, there were some exceptions. For example, a lower Hill coefficient was found for verapamil using protocol 8 (Hill coefficient = 0.55) (for voltage waveforms, refer to Fig. 1B, protocol 8), whereas, in general, Hill coefficients for terfenadine were slightly higher than 1 (e.g., the highest Hill coefficient for terfenadine was 1.67 for protocol 13) (for voltage waveforms, refer to Fig. 1B, protocol 13). These observations can perhaps be explained by factors such as the difficulty in accurately measuring the degree of block for some drugs with certain protocols. For example, the kinetics of binding of terfenadine to $K_v11.1$ have previously been shown to be problematic for measuring steady-state block, since the timecourse of block is so slow (Windley et al., 2016).

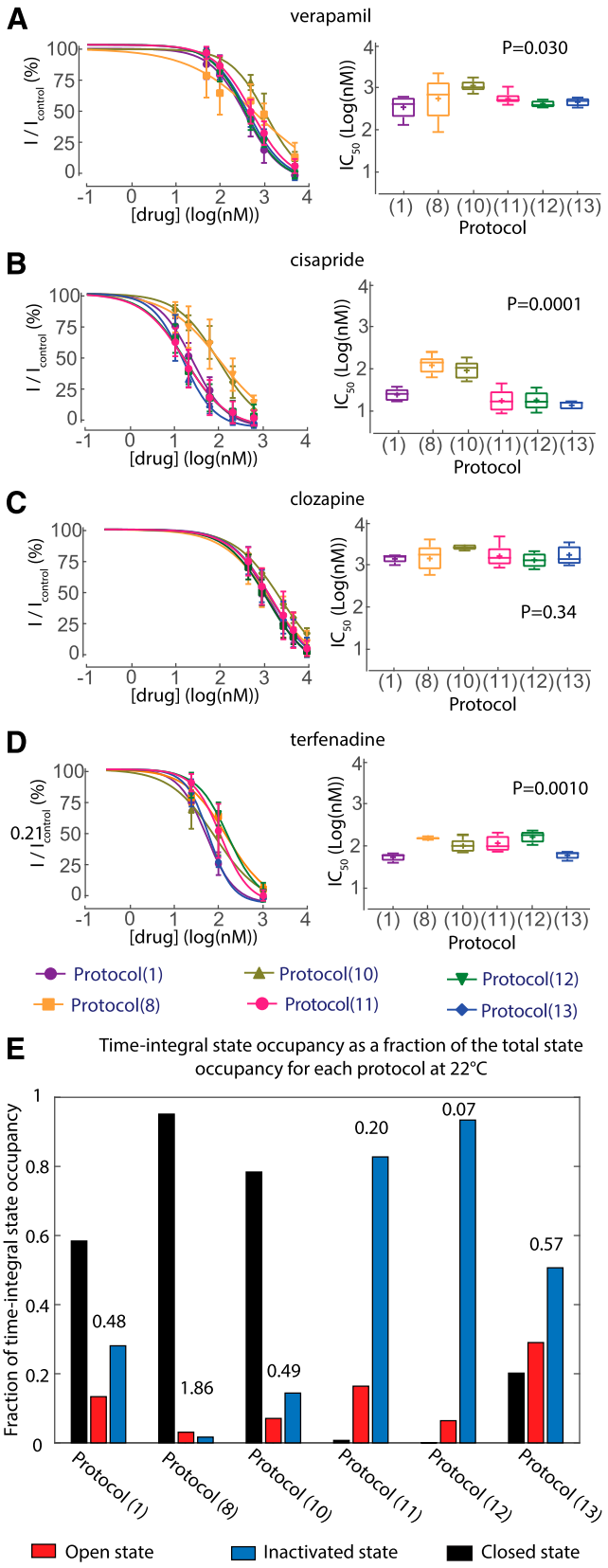

Fig. 9. In vitro experimental data. (A) Examples of in vitro K_v11.1 currents evoked when voltage clamped using voltage protocols 8 (left) and 12 (right) in the presence of increasing concentrations of drug. (A–D) Dose-response curves (left) and box plot of corresponding IC_{50} values for each of the six voltage protocols (1, 8, 10, 11, 12, and 13) (n = 4–6) in the presence of verapamil, cisapride, clozapine, and terfenadine, respectively. The central line shows the median value of each protocol. The mean for each box is depicted with a + symbol. Box plot boxes extend to the 25th and 75th percentile, of the data for each protocol, and the whiskers show the 95% confidence intervals for IC_{50} values for each protocol. P values for ANOVAs are shown for each drug. (E) Relative proportions of Fso for each of the six voltage protocols, demonstrating underlying differences in state occupancy at 22°C. The relative state occupancy (RO/I) of each protocol representing the ratio of Fso_{open} to Fso_{inact} is shown above each column in the figure.

In our experiments, an underestimation of the degree of block at low concentrations, when the timecourse of terfenadine block is slowest, would explain the Hill coefficients being greater than 1.

Predicting Potency across Different Voltage Protocols. Defining the potency of K_v11.1 block is an important part of existing preclinical safety screening, where a safety index value is determined by comparing the IC_{50} of K_v11.1 to the C_{max} of the drug (Redfern et al., 2003). However, the degree of protocol dependence of measured potency that we and others have demonstrated (Supplemental Tables 2–5), makes this is problematic because: 1) a single affinity measure does not represent a true affinity for K_v11.1—it only represents the affinity of a drug for one specific voltage protocol; and 2) even if a single voltage protocol could be agreed upon to standardize drug affinity assays, it would not adequately reflect the wide-ranging effects of external conditions such as heart rate, QT prolongation, and hypokalemia. Our data show that there is a predictable relationship between IC_{50} values measured using different protocols. Furthermore, using IC_{50} values measured from just a few simple voltage protocols, it is possible to predict what the potency of a drug will be when measured using other voltage protocols. For in silico data, this can be done with a very high degree of accuracy (Fig. 7), whereas for in vitro data, the degree of accuracy is reduced, perhaps as a result of factors such as drug trapping, which are not implicit in the Markov model used in this study. Nevertheless, this demonstration of a quantifiable relationship between the variable measured potencies of K_v11.1 block is important as it provides a framework for the direct comparison of potencies measured between groups using different assays and may allow for the reinterpretation of legacy data sets obtained using different protocols.

Prediction of State-Dependent Binding Characteristics. It has previously been shown that high-affinity binding to K_v11.1 occurs, at least for some drugs, because of preferential binding to the inactivated state (Suessbrich et al., 1997; Ficker et al., 1998; Numaguchi et al., 2000; Perrin et al., 2008a). Furthermore, preferential binding to the inactivated state has been associated with increased prolongation of the action potential duration (Lee et al., 2016), and several drugs that have been withdrawn from market (e.g., astemizole and terfenadine) or had their use severely restricted (e.g., cisapride) preferentially bind to the inactivated state (Perrin et al., 2008a). However, the quantification of state-dependent binding is difficult, since it cannot be readily measured experimentally. Rather, indirect measures relying on changes in affinity that occur as a result of perturbation of the inactivated state using site-directed mutagenesis (Suessbrich et al., 1997; Ficker et al., 1998; Numaguchi et al., 2000; Perrin et al., 2008a), changing potassium concentration (Kamiya et al., 2008), or measuring of drug-binding kinetics (Hill et al., 2014) are routinely used.

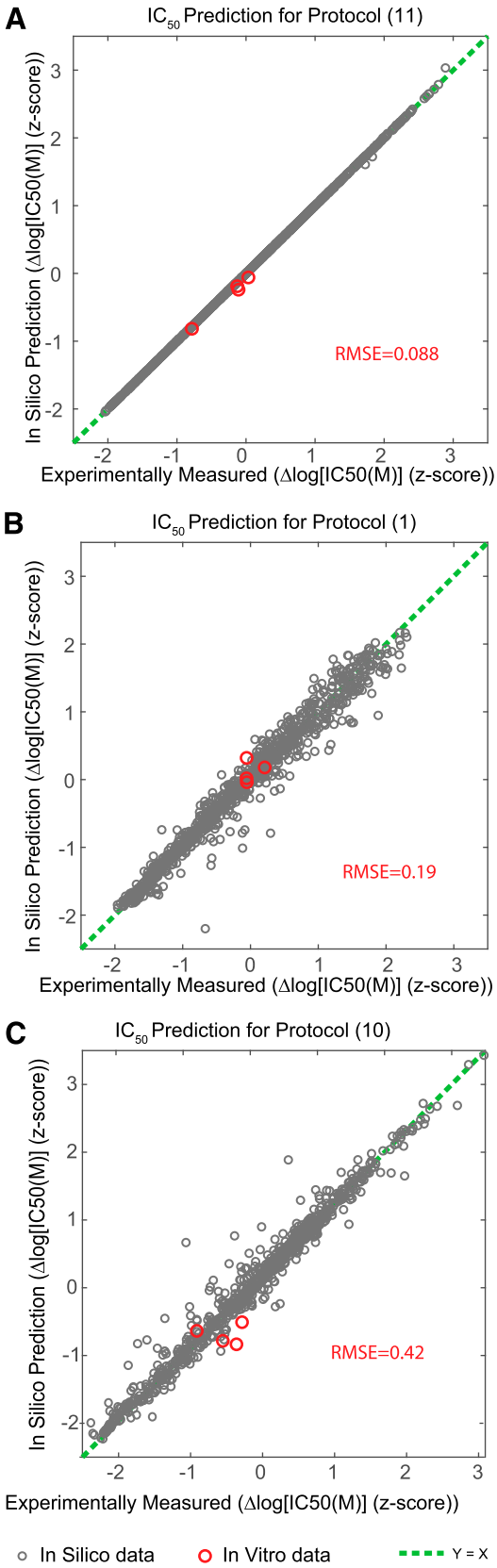

Fig. 10. In silico neural network algorithms were trained using in silico IC_{50} values from protocols 8, 12, and 13 to predict in vitro IC_{50} values for other voltage protocols using in vitro measurements of IC_{50}. For each panel, predictions vs. true measured IC_{50} value for the four in vitro drugs (verapamil, cisapride, clozapine, and terfenadine; shown in red). For context, in silico predictions from Fig. 7 are shown in gray. IC_{50} value for protocol 1 (A), IC_{50} value for protocol 10 (B), and IC_{50} value for protocol 11 (C). An identity line (Y = X) is shown as a dashed green line. The accuracy of the in vitro prediction for each of the three voltage protocols is represented as the root mean squared error (RMSE) for each panel.

In this study, we show that a machine-learning algorithm, trained using IC_{50} values measured from just three simple voltage protocols, can accurately determine the degree of state-preference drugs in silico (Fig. 6). We also used the same algorithm to predict the state preference of four drugs—clozapine, cisapride, verapamil, and terfenadine—based on our in vitro measured IC_{50} values. For clozapine, the only drug we tested for which there is a published, fully parameterized in silico model (Hill et al., 2014), meaning that the state-dependent binding properties are unambiguously known, the algorithm correctly identified this as a drug with no state preference (Table 1). For cisapride, the algorithm predicted inactivation state preference (KO/I = 0.26), consistent with previously published studies using mutagenesis, which showed a ratio of 0.37 between the IC_{50} value for wild-type $K_v11.1$ and the N588K inactivation-deficient mutant $K_v11.1$ (Perrin et al., 2008a). The data in the literature for verapamil are mixed. Previously, publications show a low variation in measured IC_{50} values from any two protocols (maximum 6-fold difference) (Supplemental Table 2), suggesting that verapamil has weak or nonpreferential state binding to $K_v11.1$. This is consistent with our model prediction of KO/I = 1.97. However, other studies have shown that potency of block of the S620T inactivation-deficient $K_v11.1$ mutant by verapamil was less potent than for wild type (Zhang et al., 1999), consistent with inactivation state preference. However, this mutation has also been shown to have a gating-independent effect on drug binding (Guo et al., 2006) (i.e., mutation at this residue directly disrupts the drug-binding site), which might confound the interpretation of the effects of this mutant in relation to state preference. Finally, our predicted KO/I for terfenadine was 69.67, suggesting a strong preference for binding to the open state of $K_v11.1$. This is inconsistent with published data using either mutagenesis (Perrin et al., 2008a) or potassium inhibition of inactivation (Kamiya et al., 2008) that identified terfenadine as a drug that preferentially binds to the inactivated state. One explanation for this is that terfenadine exhibits closed-state trapping (Kamiya et al., 2008; Windley et al., 2017), which is not accounted for in the Markov model we used, that confounds the in vitro predictions for this drug.

Limitations. The main limitations of this study, in relation to the prediction of in vitro data using an algorithm developed using in silico data, are the characteristics of the available Markov models describing drug binding to $K_v11.1$, particularly in relation to drugs that exhibit closed-state trapping. Although there are models in the literature that include either state-dependent binding (Di Veroli et al., 2013; Lee et al., 2016) or trapping (Di Veroli et al., 2014; Li et al., 2017), there are no models that include both. Development of a more complete Markov description of drug binding, which included both state-dependent binding and trapping, would further improve predictions based on in vitro data and, indeed, the quantification of state-dependent binding enabled using the approach reported here will likely facilitate the parameterization of such models.

TABLE 1

True *KO/I* compared with predicted *KO/I* for the four in vitro drug examples

Note that only clozapine has a fully parameterized model of binding to K_v11.1 from Hill et al. (2014), and therefore is the only drug that has an in vitro validated value for *KO/I*.

	True *KO/I*	Predicted *KO/I*
Verapamil	~	1.97
Cisapride	~	0.26
Clozapine	1.12	1.20
Terfenadine	~	69.97

~, value unknown.

Second, it is well known that the kinetics of drug binding to K_v11.1 channels (Windley et al., 2016) as well as the kinetics of K_v11.1 channel gating (Vandenberg et al., 2006) are temperature dependent. This is evident in the differences that we observe in the I_{Kr} current at 37°C in silico (Fig. 1B) and 22°C in vitro (Fig. 8). Ideally, therefore, an in vitro data set gathered at 37°C would be desirable for further validation. Despite this, we still achieve good prediction accuracy with our machine-learning models both for state preference and drug affinity. This is consistent with previous published data showing that even though the kinetics of drug binding to K_v11.1 for the four drugs examined here are temperature dependent, the IC_{50} values for block are not (Hill et al., 2014; Windley et al., 2016, 2018).

Conclusion. In this study, we have demonstrated that state-dependent drug binding is a major factor in determining the potency of K_v11.1 block measured using different protocols, with the exact measured potency also affected by factors such as drug-binding/drug-unbinding kinetics and closed-state trapping. As a result, we show that interprotocol differences in measured IC_{50} occur in a predictable way, meaning the potency of a compound measured using any voltage protocol can be reliably estimated from knowledge of the channel-state occupancy. This is an important step since it allows for the direct comparison of potencies measured using different assays, as well the reinterpretation of legacy data sets obtained using different protocols as part of previous compound screens. Furthermore, we also show that the state preference of a drug can be inferred from differences in its IC_{50} values measured from commonly used protocols that are simple enough to be readily deployed on high-throughout, automated patch-clamp platforms. This is the first demonstration of the quantification of state preference without the need for measuring either the kinetics of block/unblock or the disruption of K_v11.1 inactivation (using mutagenesis or ionic concentration). The ability to simply quantify state preference will facilitate the development of more complete models of drug binding to K_v11.1 and will improve our understanding of proarrhythmic risk associated with K_v11.1 blocking compounds.

Acknowledgments

The authors thank, Mark Hunter, Dr. Stewart Heitmann, and Dr. Melissa Mangala for informative discussion.

Authorship Contributions

Participated in research design: Lee, Vandenberg, Hill.

Conducted experiments: Lee, Windley, Perry.

Contributed to new reagents or analytical tools: Lee, Vandenberg, Hill.

Performed data analysis: Lee, Hill.

Wrote or contributed to the writing of the manuscript: Lee, Windley, Perry, Vandenberg, Hill.

References

Di Veroli GY, Davies MR, Zhang H, Abi-Gerges N, and Boyett MR (2013) High-throughput screening of drug-binding dynamics to HERG improves early drug safety assessment. *Am J Physiol Heart Circ Physiol* **304**:H104–H117.

Di Veroli GY, Davies MR, Zhang H, Abi-Gerges N, and Boyett MR (2014) hERG inhibitors with similar potency but different binding kinetics do not pose the same proarrhythmic risk: implications for drug safety assessment. *J Cardiovasc Electrophysiol* **25**:197–207.

Fermini B, Hancox JC, Abi-Gerges N, Bridgland-Taylor M, Chaudhary KW, Colatsky T, Correll K, Crumb W, Damiano B, Erdemli G, et al. (2016) A new perspective in the field of cardiac safety testing through the comprehensive in vitro proarrhythmia assay paradigm. *J Biomol Screen* **21**:1–11.

Ficker E, Jarolimek W, Kiehn J, Baumann A, and Brown AM (1998) Molecular determinants of dofetilide block of HERG K+ channels. *Circ Res* **82**:386–395.

Food and Drug Administration, HHS (2005) International Conference on Harmonisation; guidance on S7B nonclinical evaluation of the potential for delayed ventricular repolarization (QT interval prolongation) by Human Pharmaceuticals; availability. Notice. *Fed Regist* **70**:61133–61134.

Guo J, Gang H, and Zhang S (2006) Molecular determinants of cocaine block of human ether-á-go-go-related gene potassium channels. *J Pharmacol Exp Ther* **317**: 865–874.

Hill AP, Perrin MJ, Heide J, Campbell TJ, Mann SA, and Vandenberg JI (2014) Kinetics of drug interaction with the Kv11.1 potassium channel. *Mol Pharmacol* **85**:769–776.

Kamiya K, Niwa R, Morishima M, Honjo H, and Sanguinetti MC (2008) Molecular determinants of hERG channel block by terfenadine and cisapride. *J Pharmacol Sci* **108**:301–307.

Kirsch GE, Trepakova ES, Brimecombe JC, Sidach SS, Erickson HD, Kochan MC, Shyjka LM, Lacerda AE, and Brown AM (2004) Variability in the measurement of hERG potassium channel inhibition: effects of temperature and stimulus pattern. *J Pharmacol Toxicol Methods* **50**:93–101.

Lee W, Mann SA, Windley MJ, Imtiaz MS, Vandenberg JI, and Hill AP (2016) In silico assessment of kinetics and state dependent binding properties of drugs causing acquired LQTS. *Prog Biophys Mol Biol* **120**:89–99.

Lee W, Windley MJ, Vandenberg JI, and Hill AP (2017) In vitro and in silico risk assessment in acquired long QT syndrome: the devil is in the details. *Front Physiol* **8**:934.

Li Z, Dutta S, Sheng J, Tran PN, Wu W, Chang K, Mdluli T, Strauss DG, and Colatsky T (2017) Improving the in silico assessment of proarrhythmia risk by combining hERG (Human Ether-à-go-go-Related Gene) channel-drug binding kinetics and multichannel pharmacology. *Circ Arrhythm Electrophysiol* **10**:e004628.

Milnes JT, Witchel HJ, Leaney JL, Leishman DJ, and Hancox JC (2010) Investigating dynamic protocol-dependence of hERG potassium channel inhibition at 37 degrees C: cisapride versus dofetilide. *J Pharmacol Toxicol Methods* **61**:178–191.

Mitcheson JS, Chen J, and Sanguinetti MC (2000) Trapping of a methanesulfonanilide by closure of the HERG potassium channel activation gate. *J Gen Physiol* **115**:229–240.

Numaguchi H, Mullins FM, Johnson JP Jr, Johns DC, Po SS, Yang IC, Tomaselli GF, and Balser JR (2000) Probing the interaction between inactivation gating and Dd-sotalol block of HERG. *Circ Res* **87**:1012–1018.

O'Hara T, Virág L, Varró A, and Rudy Y (2011) Simulation of the undiseased human cardiac ventricular action potential: model formulation and experimental validation. *PLOS Comput Biol* **7**:e1002061.

Perrin MJ, Kuchel PW, Campbell TJ, and Vandenberg JI (2008a) Drug binding to the inactivated state is necessary but not sufficient for high-affinity binding to human ether-à-go-go-related gene channels. *Mol Pharmacol* **74**:1443–1452.

Perrin MJ, Subbiah RN, Vandenberg JI, and Hill AP (2008b) Human ether-a-go-go related gene (hERG) K+ channels: function and dysfunction. *Prog Biophys Mol Biol* **98**:137–148.

Potet F, Bouyssou T, Escande D, and Baró I (2001) Gastrointestinal prokinetic drugs have different affinity for the human cardiac human ether-à-gogo K(+) channel. *J Pharmacol Exp Ther* **299**:1007–1012.

Redfern WS, Carlsson L, Davis AS, Lynch WG, MacKenzie I, Palethorpe S, Siegl P, Strang I, Sullivan AT, Wallis R, et al. (2003) Relationships between preclinical cardiac electrophysiology, clinical QT interval prolongation and torsade de pointes for a broad range of drugs: evidence for a provisional safety margin in drug development. *Cardiovasc Res* **58**:32–45.

Rezazadeh S, Hesketh JC, and Fedida D (2004) Rb+ flux through hERG channels affects the potency of channel blocking drugs: correlation with data obtained using a high-throughput Rb+ efflux assay. *J Biomol Screen* **9**:588–597.

Sager PT, Gintant G, Turner JR, Pettit S, and Stockbridge N (2014) Rechanneling the cardiac proarrhythmia safety paradigm: a meeting report from the Cardiac Safety Research Consortium. *Am Heart J* **167**:292–300.

Suessbrich H, Schönherr R, Heinemann SH, Attali B, Lang F, and Busch AE (1997) The inhibitory effect of the antipsychotic drug haloperidol on HERG potassium channels expressed in Xenopus oocytes. *Br J Pharmacol* **120**:968–974.

Vandenberg JI, Varghese A, Lu Y, Bursill JA, Mahaut-Smith MP, and Huang CL-H (2006) Temperature dependence of human ether-a-go-go-related gene K+ currents. *Am J Physiol Cell Physiol* **291**:C165–C175.

Walker BD, Singleton CB, Bursill JA, Wyse KR, Valenzuela SM, Qiu MR, Breit SN, and Campbell TJ (1999) Inhibition of the human ether-a-go-go-related gene (HERG) potassium channel by cisapride: affinity for open and inactivated states. *Br J Pharmacol* **128**:444–450.

Windley MJ, Abi-Gerges N, Fermini B, Hancox JC, Vandenberg JI, and Hill AP (2017) Measuring kinetics and potency of hERG block for CiPA. *J Pharmacol Toxicol Methods* **87**:99–107.
Windley MJ, Lee W, Vandenberg JI, and Hill AP (2018) The temperature dependence of kinetics associated with drug block of hERG channels is compound-specific and an important factor for proarrhythmic risk prediction. *Mol Pharmacol* **94**:760–769.
Windley MJ, Mann SA, Vandenberg JI, and Hill AP (2016) Temperature effects on kinetics of KV11.1 drug block have important consequences for in silico proarrhythmic risk prediction. *Mol Pharmacol* **90**:1–11.
Wu W, Gardner A, and Sanguinetti MC (2015) The link between inactivation and high-affinity block of hERG1 channels. *Mol Pharmacol* **87**:1042–1050.
Yao J-A, Du X, Lu D, Baker RL, Daharsh E, and Atterson P (2005) Estimation of potency of HERG channel blockers: impact of voltage protocol and temperature. *J Pharmacol Toxicol Methods* **52**:146–153.
Zhang S, Zhou Z, Gong Q, Makielski JC, and January CT (1999) Mechanism of block and identification of the verapamil binding domain to HERG potassium channels. *Circ Res* **84**:989–998.

Address correspondence to: Adam P. Hill, Molecular Cardiology and Biophysics Division, Victor Chang Cardiac Research Institute, 405 Liverpool Street, Darlinghurst 2010, NSW, Australia. E-mail: a.hill@victorchang.edu.au